Diffusion in Intact Secondary Cell Wall Models of Plants at Different Equilibrium Moisture Content

Daipayan Sarkar[1], Lintao Bu[2], Joseph E. Jakes[3], Jacob K. Zieba[4], Isaiah D. Kaufman[4], Michael F. Crowley[2], Peter N. Ciesielski[2], Josh V. Vermaas[1,4,*]

[1]MSU-DOE Plant Research Laboratory, Michigan State University, East Lansing MI 48824
[2]Renewable Resources and Enabling Sciences Center, National Renewable Energy Laboratory, Golden, CO 80401
[3]Forest Biopolymers Science and Engineering, USDA Forest Service, Forest Products Laboratory, Madison, WI, 53726
[4]Biochemistry and Molecular Biology, Michigan State University, East Lansing MI 48824

* Corresponding author: vermaasj@msu.edu

Abstract

Secondary plant cell walls are composed of carbohydrate and lignin polymers, and collectively represent a significant renewable resource. Leveraging these resources depends in part on a mechanistic understanding for diffusive processes within plant cell walls. Common wood protection treatments and biomass conversion processes to create biorefinery feedstocks feature ion or solvent diffusion within the cell wall. X-ray fluorescence microscopy experiments have determined that ionic diffusion rates are dependent on cell wall hydration as well as the ionic species through non-linear relationships. In this work, we use classical molecular dynamics simulations to map the diffusion behavior of different plant cell wall components (cellulose, hemicellulose, lignin), ions (Na^+, K^+, Cu^{2+}, Cl^-) and water within a model for an intact plant cell wall at various hydration states (3 – 30 wt.% water). From these simulations, we analyze the contacts between different plant cell wall components with each other and their interaction with the ions. Generally, diffusion increases with increasing hydration, with lignin and hemicellulose components increasing diffusion by an order of magnitude over the tested hydration range. Ion diffusion depends on charge. Positively charged cations preferentially interact with hemicellulose components, which include negatively charged carboxylates. As a result, positive ions diffuse more slowly than negatively charged ions. Measured diffusion coefficients are largely observed to best fit piecewise linear trends, with an inflection point between 10-15% hydration. These observations shed light onto the molecular mechanisms for diffusive processes within secondary plant cell walls at atomic resolution.

1. Introduction

Wood and other forms of lignocellulosic biomass constitute an abundant natural resource with a tremendous capacity to provide sustainable fuels, chemicals, and materials for a variety of applications (Zhu et al., 2016). Biorefineries seek to employ conversion strategies to deconstruct lignocellulosic biopolymers into smaller molecules that can be subsequently converted into fuels or platform chemicals, recreating the petrochemical products with a smaller temporal gap between photosynthesis and utilization (Cherubini, 2010; de Jong and Jungmeier, 2015). These conversion strategies employ biochemical processes such as enzymatic hydrolysis and fermentation, and thermochemical pathways such as pyrolysis and catalytic upgrading, to drive transformation of biomass-derived molecules into desirable products. Wood is also intrinsically valuable as a sustainable construction material for a wide range of applications, including furniture, tools, and buildings (Jakes et al., 2016). More recently, mass timber products like cross-laminated timber panels have been developed and become viable alternatives to nonrenewable steel and concrete materials for the construction of mid- to high-rise buildings (Brandner et al., 2016).

Understanding and controlling transport of ions and small molecules throughout wood and lignocellulosic biomass is critical to both biorefining and materials applications. For example, biological conversion scenarios use thermochemical pretreatments to enhance the yields of enzymatic hydrolysis (Kothari et al., 2018; Xu et al., 2016). Such pretreatments involve infiltration of the biomass with mineral acids and bases such as sulfuric acid and sodium hydroxide, which diffuse into cell walls to depolymerize non-structural polysaccharides and thereby provide better access for cellulase enzymes during saccharification (Mosier et al., 2005). Similarly, biomass fractionation processes often require diffusion of small molecular solvents into the cell walls to enable extraction of select biopolymer components (Thornburg et al., 2020).

For construction material applications, transport processes through woody cell wall materials is also important for creating durable adhesive bonds (Hunt et al., 2018a), chemically modifying wood (Hill, 2006; Plaza et al., 2022), and wood preservation treatments (Ibach et al., 2022; Kirker and Lebow, 2021). Wood degradation mechanisms, such as fungal decay (Ibach et al., 2022; Kirker et al., 2017) and metal fastener corrosion (Zelinka et al., 2019, 2010), are also controlled by transport. These types of degradation limit the utility of wood in high moisture environments. An improved understanding of transport mechanisms would accelerate the development of more environmentally friendly wood preservation treatments and improved resistance to degradation, thereby expanding the market for sustainable wood construction materials (Falk, 2009).

Wood tissue exhibits a hierarchical structure which provides structural support while enabling transport of water and nutrients (Arzola-Villegas et al., 2019). The microstructure is highly porous and varies extensively between species. Bulk transport of water and ions is effectively facilitated by the macroporosity of wood (Fredriksson et al., 2022), however intra-cell wall diffusion requires infiltration into the complex assembly of lignocellulosic polymers. Quantitatively discerning the precise nanostructure of lignocellulosic biomass is still an active area of research (Kirui et al.,

2022; Perras et al., 2017); however, it is generally accepted that bundles of several dozen cellulose chains are assembled into larger fibrils which are decorated with hemicellulose and further ensheathed with lignin (Kirui et al., 2022; Lyczakowski et al., 2019), and that the internal structure and dynamics change as a function of hydration (Paajanen et al., 2022).

Many studies have investigated molecular transport within wood and other types of biomass with computational (Chen et al., 2019; Shi and Avramidis, 2021) and experimental (Jakes, 2019; Jakes et al., 2020; Zelinka et al., 2015) methods. Given suitable structural characterization of the macroporosity of wood tissue, often by imaging methods, bulk transport throughout the interconnected pores can be well-described by direct numerical simulation considering the structure explicitly, and coupling this structure to reduced order approximations for bulk transport in porous media (Autengruber et al., 2020; Thornburg et al., 2020). However, characterizing diffusive transport within the cell wall has proven far more challenging largely because the length scale at which intra-cell wall diffusion occurs (~ 10^{-5} m) and the difficulty of decoupling intra-cell wall diffusion from bulk diffusion through the macropores precludes most bulk measurement techniques. From a materials perspective, unmodified lignocellulosic cell walls are solid polymers and intra-cell wall transport is expected to be a solid polymer diffusion process (Jakes et al., 2019), with motions at the atomic scale by the individual polymers in the cell wall together with hydration levels controlling diffusion.

Recent experimental work on latewood loblolly pine cell wall layers strongly supports that diffusion through unmodified wood cell walls is a solid polymer diffusion process, where motions within the polymer structure are limiting to transport. Using synchrotron X-ray fluorescence microscopy (XFM) and a custom-built RH chamber, Zelinka and coworkers directly observed that there is a 60-85% RH threshold for mineral ion diffusion in individual wood cell wall layers (Zelinka et al., 2015). At levels below this level of hydration, there is simply no room in the wood nanostructure to permit diffusion, whereas enough water intercalates into the wood structure at greater humidity to plasticize the wood polymers and facilitate mineral ion diffusion. Interestingly, the 60-85% RH range also corresponds to the 50-85% RH range for the moisture-induced glass transition in amorphous polysaccharides (Jakes et al., 2019; Paajanen et al., 2022). Using nanoindentation dynamic mechanical analysis, it is possible to assess the moisture- and time-dependence of the molecular relaxations corresponding to the glass transition (Jakes, 2019). These molecular relaxations correlate directly to ionic conductivity measurements made on similar wood cell wall layers, demonstrating that ionic conductivity is being controlled by the molecular relaxations (Jakes, 2019). This manifests concretely in time-lapse XFM imaging, from which it is possible to determine moisture-dependent ion diffusion constants (Jakes et al., 2020). The direct connection to moisture content highlights how structural changes at the atomic scale propagate forward to higher order observables.

With this experimental context in mind, the current study aims to use the power of molecular simulation to act as a computational microscope to identify how interactions in intact biomass respond to changes in hydration (Figure 1). Using prior experiments as a benchmark for comparison (Jakes et al., 2020), we can compute diffusion coefficients for multiple ion species (Na^+, K^+, Cu^{2+}, and Cl^-) within our models. We find that the diffusion coefficients determined from

atomistic simulation models show the same trends found experimentally. Using the detailed structural information available only from an atomic model, we find that increasing hydration reduces contacts between individual biopolymers within a cell wall, creating the space for rapid diffusion along hydrated tracks parallel to the hemicellulose strands once water molecules account for 10-15% of the total mass for the cell wall. The detailed molecular picture also identifies interactions between carboxylate groups that decorate the hemicellulose and positive ions. These interactions impede diffusion even further beyond what the crowded conditions require within the cell wall.

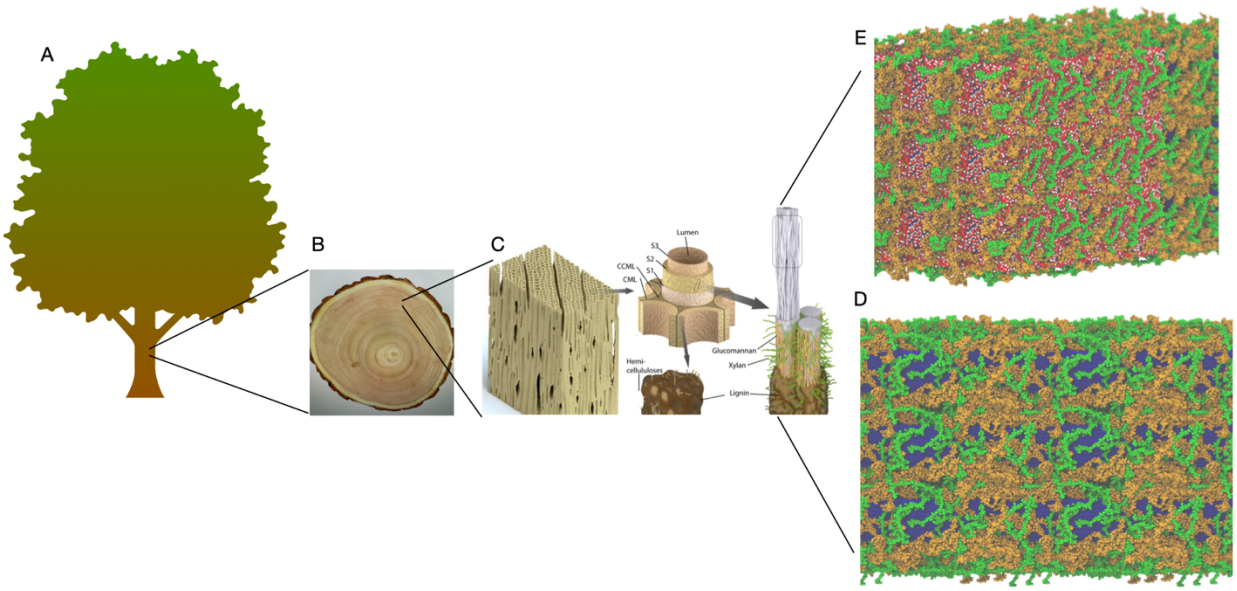

Figure 1: Hierarchical anatomy of a tree. (A) Macroscale illustration of a tree (B) cross-section of a tree trunk, showing the rings and bark (C) Illustration showing the breakdown for softwood from micro to nanoscale. The secondary cell walls are indicated by S1, S2 and S3 and the cells are adhered to each other by the compound middle lamella (CML). The secondary cell wall also consists of hemicellulose labeled as xylans (green) and lignin (brown) (D) All-atom model for a plant cell wall with cellulose (blue), hemicellulose (green) and lignin (orange) (E) All-atom model for the plant cell wall with 30 wt.% water. In this representation oxygen in water molecules is shown as red and the hydrogens are represented by white colors. Sub-panel figure (C) is reproduced with permission from (Jakes et al., 2020) under the Creative Commons Attribution 4.0 International License.

2. Materials and Methods

2.1 Atomistic model of plant secondary cell wall

The secondary cell wall model used here contains the three major polymers, cellulose, hemicellulose, and lignin, in approximately the ratio found in hardwood (Walker, 2006) (Table 1). The cellulose model contains four 18-chain cellulose I_β bundles with DP (degree of polymerization) of 40 in the 234432 motif (Langan et al., 2005) (Figure 2). Decorated xylan molecule with DP of 40 was used to represent hemicellulose. Experimental studies suggest that ~40-70% of the xylose residues are acetylated on C_2 or C_3 positions and D-glucuronic acid groups are also linked to C_2 or C_3 in ~10% of the xylose residues (Walker, 2006). In our xylan model, the

D-glucuronic acid groups are linked to C_2 in every one of eight xylose residues, whereas the acetyl groups are linked to C_2 in every other xylose residue. In models where the C_2 has been occupied by a D-glucuronic acid group, the acetyl group is linked to C_3. All the substitution groups are located on the even-numbered xylose residues, leading to a xylan molecule with all decorations on the same side (Figure 2). A schematic lignin 20-mer model proposed by (Ralph et al., 2019) for hardwood was used to construct the structure of the lignin polymer model, which contains 13 syringol units and 7 guaiacol units (S:G = 65:35) (Figure 2). While the individual polymers were repeated to fill the simulation volume (Table 1), and therefore the polymer distribution is not polydisperse like it would be in intact biomass, the system approximately represents intact biomass to within the limitations of current modeling approaches. The individual components were assembled using PACKMOL (Martínez et al., 2009) into a rectangular simulation volume. The generated PCW model was compressed slowly by decreasing the simulation box dimensions until a desired density of 1.5 g/cm^3 determined experimentally from dried wood (Zauer et al., 2013) was achieved at a box size of 78.8 Å x 78.8 Å x 210.6 Å. Sodium ions were added to maintain the total charge of the system to be neutral.

Table 1 summarizes the composition of the PCW model constructed in this work. The 30 xylan molecules with a 2-fold conformation and the 58 lignin molecules were randomly placed surrounding the four cellulose bundles using the PACKMOL program.

Table 1. Composition in the plant secondary cell wall model.

	Experimental Composition	Experiment ratio (weight)	DP of biopolymer	Number of chains	Simulation ratio (weight)
Cellulose	45%	2.25	40	72	2.20
Xylan	20%	1.00	40	30	1.00
Lignin	25%	1.25	20	58	1.22

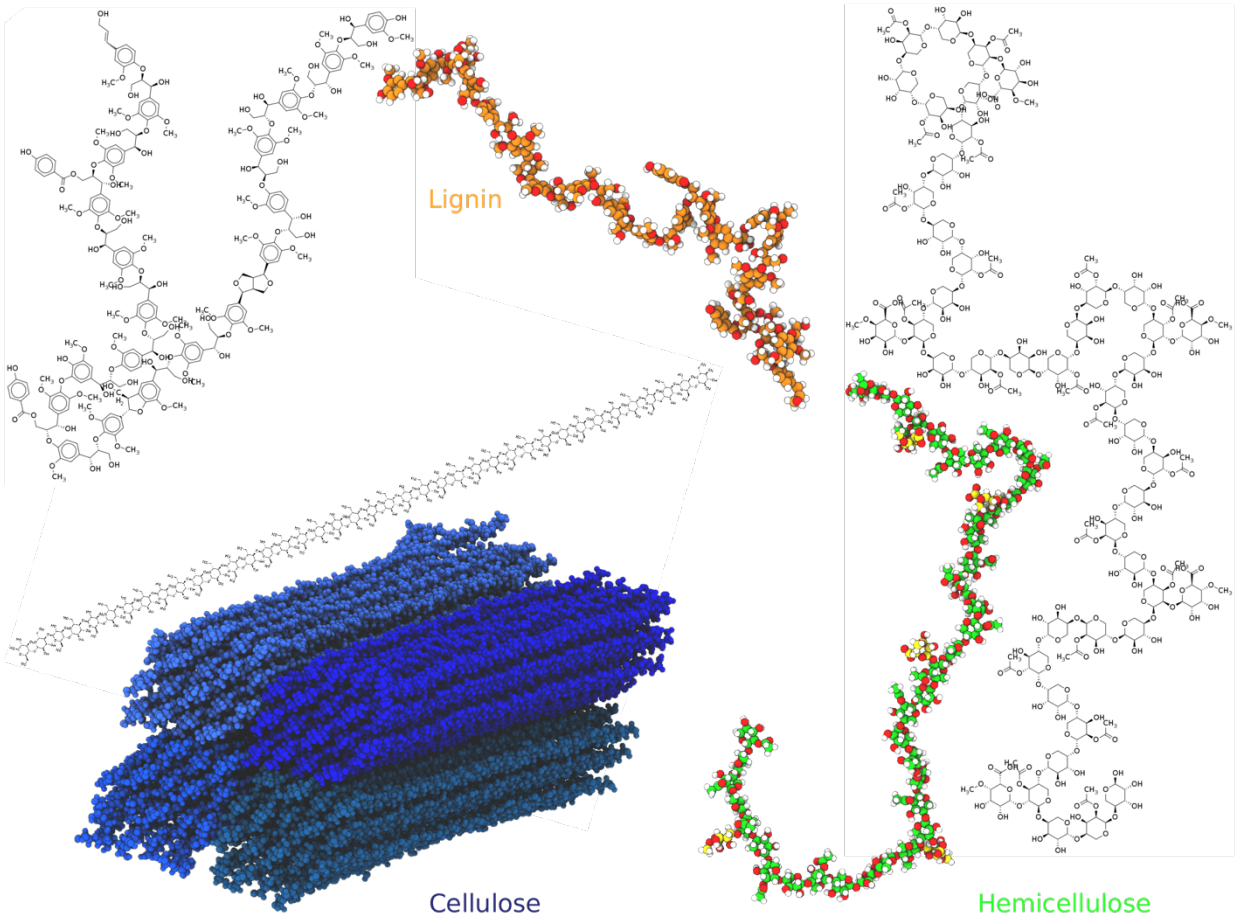

Figure 2: Chemical structures and corresponding atomic model for a single fragment of secondary cell wall polymers hemicellulose (green) and lignin (orange), alongside cellulose microfibrils (shades of blue, representing the 4 cellulose bundles). There are total of 72, 30, and 58 copies of cellulose, hemicellulose, and lignin polymers in our atomic secondary cell wall model. The chemical structures made using Marvin Sketch 22.16.

2.2 Complete the model with water and ions

The initial model described above was generated such that water was 3 weight percent of the total simulation system. To generate alternative systems with different hydration levels, the hemicellulose and lignin polymers were moved such that the center of geometry each individual molecule was multiplied by a constant factor, effectively moving each polymer away from cellulose fibril without introducing ring penetrations. Additional water molecules were added into the interstitial spaces after rewrapping the lignocellulose using the solvate plugin to VMD. By empirically varying the constant factor by which the system was expanded, we obtain models that are 0, 3, 5, 10, 15, 20, 25, or 30 percent water by weight (100% x mass water / mass total) (Figure 3) and range from approximately 120,000 atoms to 190,000 atoms in size. Converting to equilibrium moisture content, these systems have an equilibrium moisture content of 0, 3.1, 5.3, 11.7, 17.6, 25.4, 33.4, and 43.9%, respectively. This range of hydration spans hygroscopic

measurements for wood at across all humidity levels up to the fiber saturation point (Glass et al., 2014).

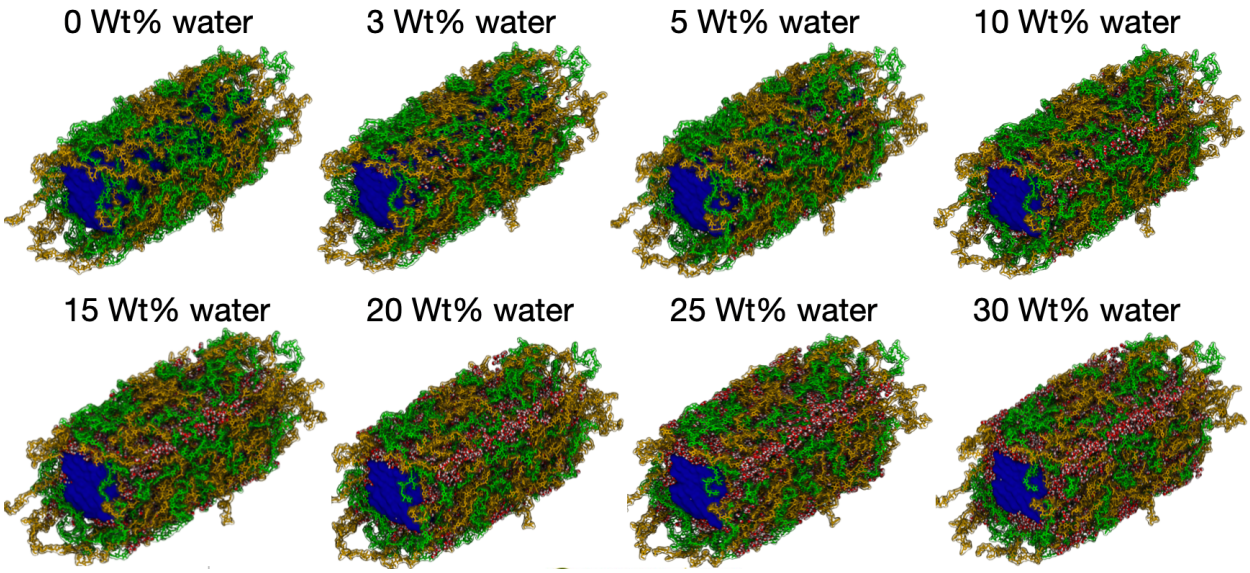

Figure 3: Atomistic representation of secondary cell wall in plants at different moisture levels. In this representation, blue is used for the central cellulose fibril, orange for lignin polymers, and green for hemicellulose. Atoms within a water molecule are color coded, with red for oxygen and white for hydrogen. The range 0 – 30% of water weight percent represents low to high moisture content in wood.

To track ion diffusion within the system, ions were added by replacing water molecules within the system. Three ionization models were prepared for each level of hydration, shown in Figure 3. In the first case, only neutralizing sodium ions were added to each model. To directly compare against experimental findings, 100mM KCl, and $CuCl_2$ salts were added to the hydrated neutralized models using the autoionize plugin to VMD to create two alternative systems.

2.3 Molecular Dynamics

The 22 models were minimized briefly using NAMD 2.14 (Phillips et al., 2020) to prepare for production simulations using the GPU resident integrator in NAMD 3.0a9 (Phillips et al., 2020). The fourteen systems ionized with KCl and $CuCl_2$ were simulated for 400ns to determine the diffusion coefficient for these ions within the cell wall. The eight systems where the model was only neutralized were simulated for 1000 ns to assess for structural changes that may take longer to manifest.

Other simulation parameters are shared. The CHARMM36 force field was used to describe interactions between carbohydrates (Guvench et al., 2009, 2008; Hatcher et al., 2009), lignin (Vermaas et al., 2019), water (Jorgensen et al., 1983), and ions (Beglov and Roux, 1994). Following CHARMM36 standards, we used a 12 Å cutoff and a force switching function after 10 Å. Long range electrostatics was treated using particle mesh Ewald with a 1.2 Å grid spacing (Essmann et al., 1995). To enable a 2fs timestep between force evaluations, covalent bonds to hydrogen

atoms were treated using the RATTLE algorithm (Miyamoto and Kollman, 1992). The Langevin thermostat was set to maintain a temperature of 300K using a $5ps^{-1}$ damping coefficient (Paterlini and Ferguson, 1998). A Langevin barostat semi-isotropic with respect to the cellulose fibril axis was set to maintain 1 atm pressure (Feller et al., 1995).

2.4 Analysis

In the analysis of our trajectories, we quantified key observables such as diffusion coefficients and intermolecular contacts using scripts written for python-enabled alpha versions of VMD 1.9.4 (Humphrey et al., 1996). Leveraging python libraries such as NumPy (Harris et al., 2020), SciPy (Virtanen et al., 2020), and matplotlib (Hunter, 2007), we use Einstein's relation to quantify diffusion from the mean-squared displacement (Einstein, 1905). To analyze diffusion, we leverage the long trajectories by analyzing multiple 50ns trajectory snippets to determine a diffusion distribution. In this analysis, the trajectories are aligned to the cellulose fibril to eliminate drift based on thermostat fluctuations and the initial velocities. The diffusion coefficient within an individual snippet is determined from the slope of the linear fit between mean squared displacement and time ($D = \frac{MSD(t)}{6t}$), ignoring the fit to the first 5 ns of data. This procedure enables multiple samples to be taken from a single trajectory, facilitating error estimation.

In addition to diffusion, we also track and quantify contacts between different polymers over time. Rather than using a rigid cutoff, we evaluate contacts between heavy atoms using a sigmoid function, first used in (Sheinerman and Brooks, 1998) to describe native contacts within a protein.

$$C_{ij} = \sum_{i,jpairs} \left[1 + e^{-5\text{Å}^{-1}(4\text{Å} - d_{ij})}\right]^{-1} \quad (1)$$

This contact sum captures the essential close-contact interactions between cell wall components and is less sensitive to an arbitrary cutoff choice than other alternative metrics. To determine the contact number in the dense, periodic system, we used the KDtree implementation in Scipy (Virtanen et al., 2020) to determine contact distances between atoms within the periodic system using a minimum image convention.

3. Results

Here, we present the results from independent all-atom molecular dynamics (MD) simulations of the plant secondary cell wall (Animation S1) with different water weights, ranging from 0 – 30 wt% water, which span the realistic range for wood moisture content. First, we calculate the diffusion coefficient (D) of cell wall polymers, ions, and water at different water weights. In addition, we calculate the diffusion coefficient of ions (Na^+, K^+, Ca^{2+}, Cl^-) in the cell wall and find that our results agree well with previously reported X-ray fluorescence microscopy measurements (Jakes et al., 2020). Next, we quantify the contacts between different cell wall polymers using Eq. 1. Both molecular diffusion and measured contacts between cell wall polymers exemplify changes in the mechanical properties of secondary cell wall at varying moisture levels.

3.1 Diffusion of plant secondary cell wall components

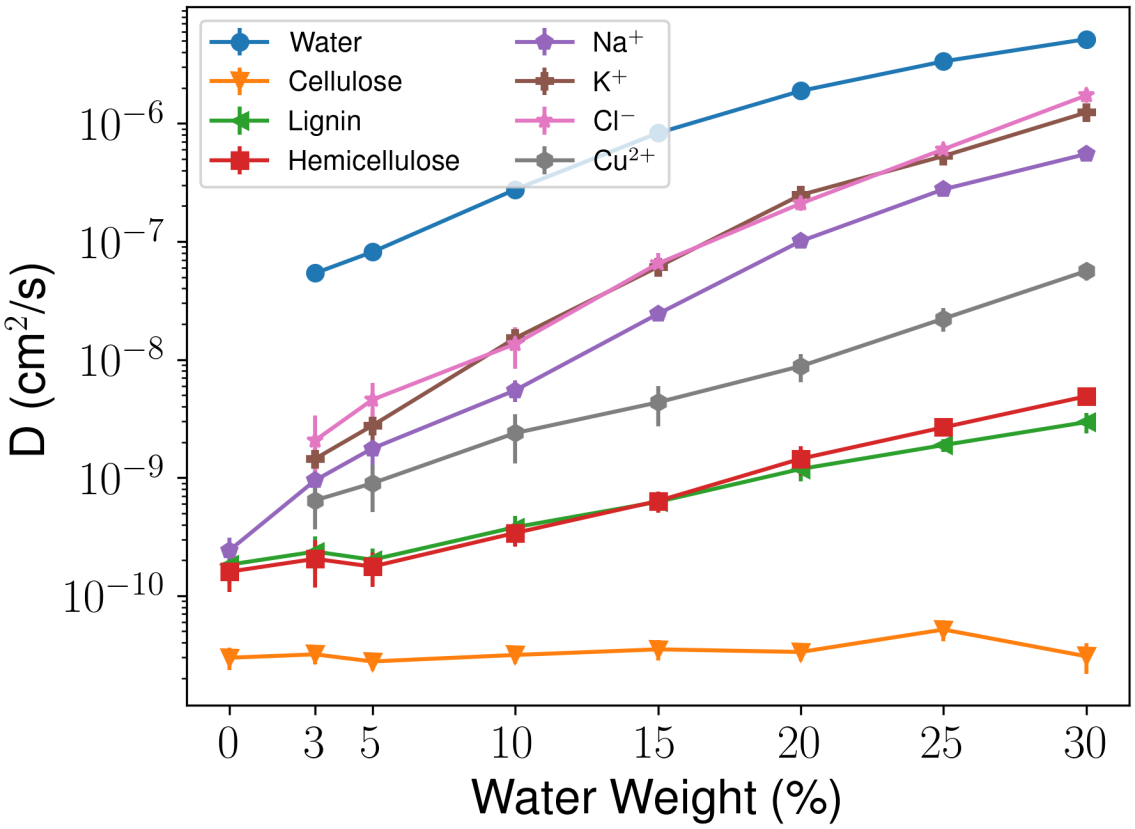

Figure 4: Diffusion of different cell wall components and ions within the network formed by the secondary cell wall in woody plants as function of different moisture content. As detailed in the methods, diffusion coefficients were determined via Einstein's relation using independent 50 ns snippets for the 1000 ns (water, cellulose, lignin, hemicellulose, and neutralizing Na^+) or 400 ns trajectories (other ions). The standard error estimates are derived from the 20 or 8 independent 50 ns samples gathered from the full trajectory.

Visually, the increase in diffusion is immediately apparent from our trajectories. As shown in supporting animation S2, cell walls with low moisture content appear to be essentially static over the microsecond long trajectory animations. By contrast, increasing hydration creates trajectories that are visibly more dynamic (Animation S3), even if the overall structure remains relatively consistent over the simulation timescale.

The measured diffusion rates across the different cell wall models vary considerably and are dependent on hydration within the plant cell wall (Figure 4). Higher moisture content is observed to broadly increase diffusion by more than an order of magnitude across the hydration levels tested. Following general trends for diffusion in solution, larger polymers diffuse more slowly than ions or water, and ions move more slowly than the water molecules that lubricate the interpolymer spaces within the model.

The water within the model exhibits slower dynamics than it would in bulk solution. Whereas the expected diffusion coefficient for the TIP3 water model is 6 x 10^{-5} cm^2/s (Mark and Nilsson, 2001), we find that water diffusion within the confines of the cell wall is at least an order of magnitude slower (Figure 4). Slower water dynamics compared to bulk with a similar order of magnitude difference have been observed previously through quasielastic neutron scattering measurements (Plaza Rodriguez, 2017).

Among the cell wall polymers, cellulose is observed to have the slowest diffusion (Figure 4). The cellulose fibril is on aggregate the largest single entity in the simulation system at approximately 470 kDa. Its size and slow motion made cellulose the natural choice for aligning the overall trajectory prior to measuring the mean squared displacements needed to calculate the diffusion coefficients reported in Figure 4. Without this realignment, correlated drifts for the center of mass of the whole system pollute the diffusion measurement, substantially accelerating diffusion for the slowest components. The lignin and hemicellulose fractions have similar diffusion profiles, owing to the similar molecular weights for each individual molecule within the system, 4.5kDa for lignin fragments, and 7.1 kDa for each hemicellulose chain. However, size is not the only determinant for diffusion, as hydrophilic hemicelluloses demonstrate slightly larger gains in diffusion coefficient with increasing hydration than amphipathic lignin polymers do. The exception to this is cellulose, which is the largest single polymer component within the cell wall model and was used as the reference to eliminate center of mass drift from the trajectory.

3.2 Ion diffusion in secondary cell wall of plants

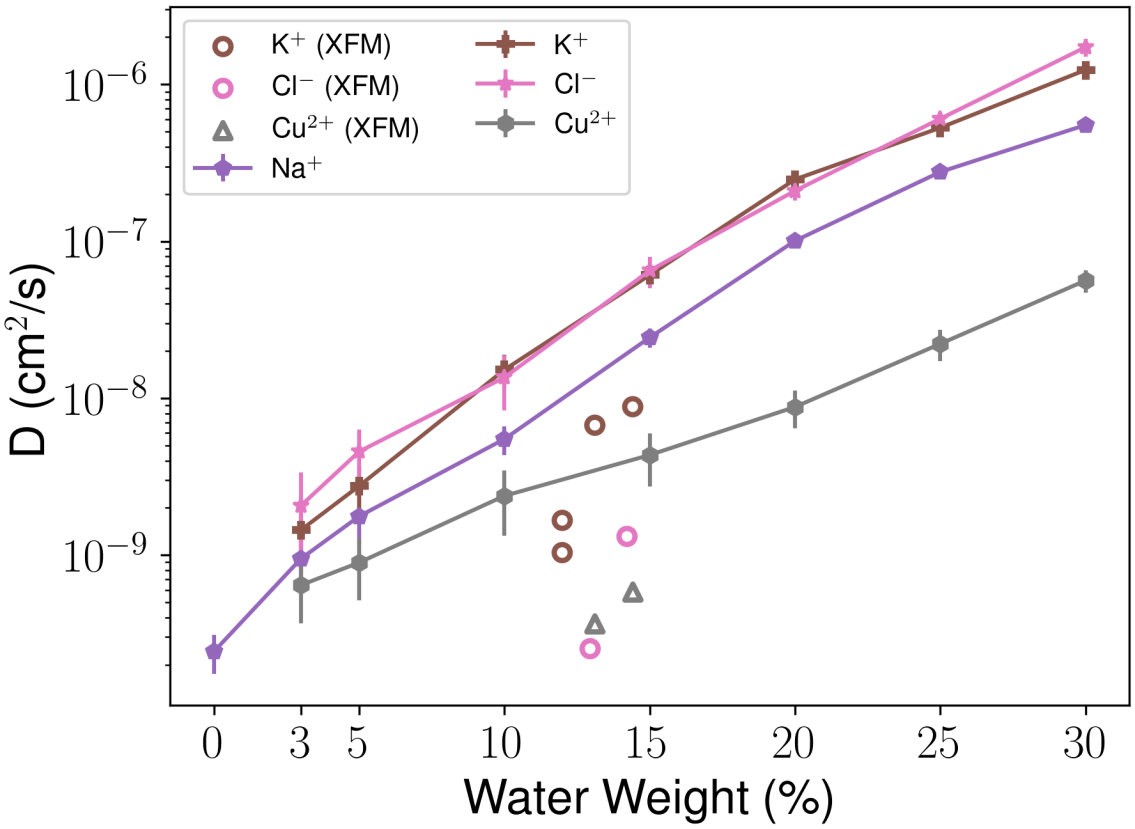

Figure 5: Ion diffusion as a function of moisture index in secondary cell wall of woody plants. We calculate the diffusion of cations (Na^+, K^+ and Cu^{2+}) and anion (Cl^-). Overall, ion diffusion increases as the moisture index increases. For KCl and $CuCl_2$ at 0.1 M initial concentration, diffusion coefficients were previously measured using time-lapse X-ray fluorescence microscopy (XFM) (Jakes et al., 2020). Scatter circles and triangles with no face color represent the experimental data for the respective cation (K^+ and Cu^{2+}) and anion (Cl^-). Atomic level molecular diffusion agrees within an order of magnitude with microscale scale diffusion measurements. Similar to observations reported in XFM experiments, we find in MD simulations that K^+ diffuses faster than Cu^{2+} ions.

To tie the diffusion results to reality, we can compare ion diffusion coefficients from within our model directly to diffusion coefficients determined from time-lapse X-ray fluorescence microscopy (XFM) experiments (Jakes et al., 2020). Figure 5 reports the diffusion of ions calculated from MD simulations, replicating information from Figure 4, and directly compares the measured diffusion with the imputed diffusion coefficients from XFM. The time-lapse XFM ion maps were collected in a preconditioned 2 µm thick section of loblolly pine (*Pinus taeda*) held at 70%, 75%, or 80% relative humidity, which is 14 – 16% equilibrium moisture content (Glass et al., 2014). The diffusion determined via simulation is approximately one order of magnitude faster than the experimental references. Multiple factors may contribute to this discrepancy. On the technical side, the selected water model within our simulation system is known to have faster diffusion by roughly a factor of two, with a diffusion coefficient of approximately 4-6 x 10^{-5} cm^2/s depending on temperature rather than 2.3 x 10^{-5} cm^2/s (Mark and Nilsson, 2001). Likewise, the

initial ion distribution is different between the homogenous initial distribution from the simulation compared with the ion wavefront from a single source that was tracked in XFM. Since local charge neutrality needs to be maintained, both cations and anions diffuse at similar rates as measured by XFM (Jakes et al., 2020), but can move independently in the periodic simulation volume. This is seen mostly explicitly in the Cl anions (Cl^-), which diffused as similar rates regardless of counterion in simulation but exhibited diffusion that matched the associated cation measured with XFM (Jakes et al., 2020). Together, we anticipate that the coupled nature of diffusion in XFM would slow diffusion of the wavefront relative to a tissue already impregnated with ions. Since we recapitulate the key trends found experimentally, that K^+ diffuses much more rapidly than Cu^{2+} (Figure 5), with magnitudes that are reasonable given the different conditions seen between the two experiments, our simplified cell wall model recapitulates the essential dynamics of ion permeation into cell walls.

Having established the correspondence with experiment, the widely varying water content from simulation can be used to establish trends over a wide range of conditions, including those that may be inaccessible experimentally. We observe that the diffusion coefficient of inorganic ions increases with the water weight in the cell wall of woody plants. At low water weight, akin to low moisture content, the diffusion is slow (~ 10^{-9} cm^2/s) but grows by almost three orders of magnitude (10^{-6} cm^2/s) for wood with 30 wt.% water. The wide range observed in the diffusion of ions can be attributed to the interactions between inorganic ions and the local secondary cell wall environment with different water weights. As the water weights increase, the ions appear in a more hydrated environment, and diffusion approaches values observed for bulk diffusion in solution.

The diffusion for individual ions appears to be related to the hydration shell radius. Within the MD simulation trajectories, we observe that similarly charged ions may have different diffusion coefficients. For instance, the sodium ion (Na^+) diffusion is a factor 2-3 slower compared to potassium ion (K^+) (Figure 5). This correlates with measures of the hydration shell radius, as measures for K^+ (3.31 Å) or Cl^- (3.32 Å) are similar, followed by Na^+ (3.6 Å) and then Cu^{2+}, which has a larger hydration shell (4.1 Å) (Jakes et al., 2020). This relationship mechanistically suggests that rapid ion diffusion depends on solvating the ion within the relatively mobile water within the cell wall environment.

3.3 Contacts between secondary cell wall components

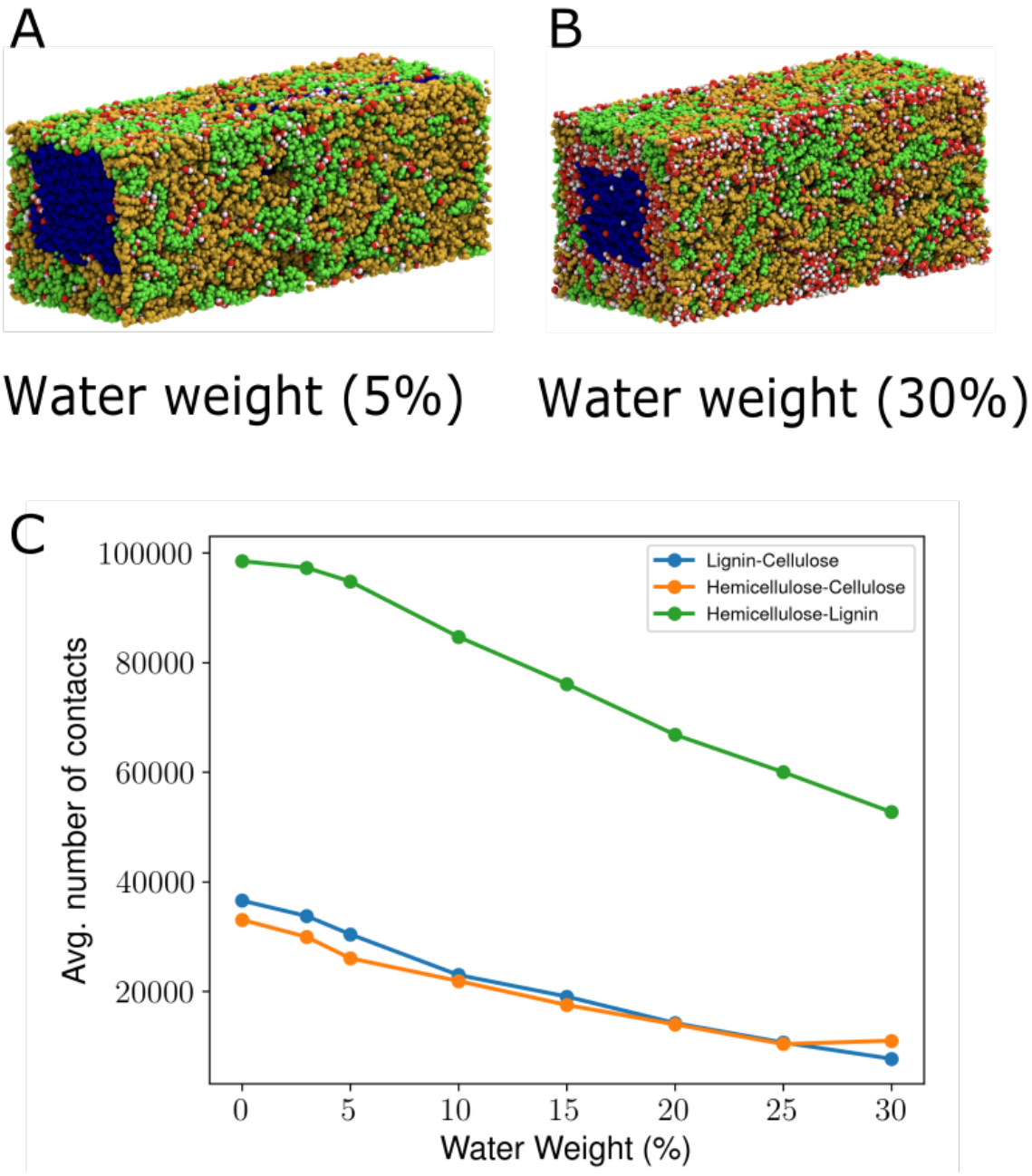

Figure 6: Quantifying average contact between cell wall components at different water weights (A, B) Atomistic models illustrating low and high moisture content, 5% and 30% water weights respectively in secondary cell wall in plants. In this figure, the cellulose microfibril is represented in blue, hemicellulose in green and lignin in orange. To maintain the same aspect ratio for the systems represented in panels (A) and (B), panel A is zoomed in further due to the smaller dehydrated system. The water is represented by red (oxygen atom) and white (two hydrogen atoms). (C) The average number of contacts between individual cell wall components – cellulose, hemicellulose, and lignin. The average number of contacts reduces as the moisture level

increases, as water molecules diffuse in between the spaces impeding interaction between individual components.

Figures 6A and 6B represent a molecular system of the plant secondary cell wall at low and high moisture content, 5 and 30 water weight percent respectively. Even after extensive equilibration under constant pressure conditions, we see that there may be large voids in between individual cell wall components. This is particularly true for models with lower water content, as water can more readily fill in gaps within the cell wall structure for hydrated cell walls. As a consequence, close contacts between different cell wall polymers goes down with increasing hydration (Figure 6C). By hydrating the system and removing interpolymer contacts, water acts as a lubricant to polymer motion within the cell wall. Fundamentally, the reduction in contacts demonstrated by Figure 6C drives the increase in biopolymer motion first characterized in Figure 4. Figure 6C also demonstrates why cellulose-hemicellulose and especially cellulose-lignin interactions have been historically so difficult to quantify, since there are just many more hemicellulose-lignin interactions, even in the absence of covalent linkages between the polymers.

3.4 Interactions between ions and plant cell wall components

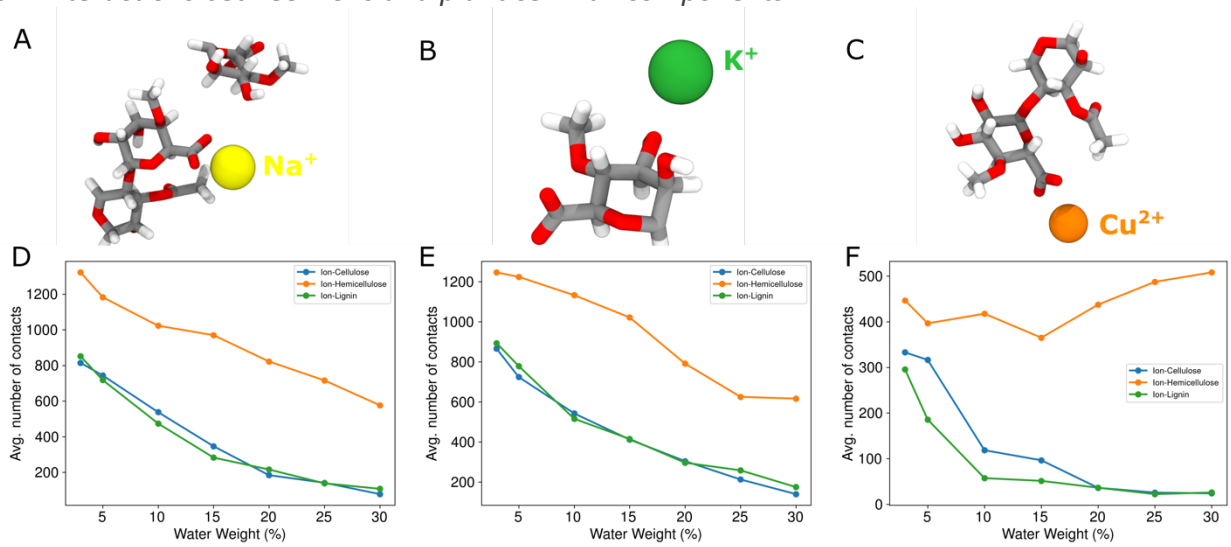

Figure 7: Interaction between ions and individual polymers in plant secondary cell wall (cellulose, hemicellulose, and lignin). The different cations used in this study are Na^+ (yellow), K^+ (green) and Cu^{2+} (orange) and snap shots of their interactions with the carboxylate functional group in hemicellulose shown in sticks with gray, red and white colors representing the carbon, oxygen, and hydrogen atoms respectively. Ion interaction reduces with increase in moisture content. Interaction between ions and hemicellulose are always higher compared to the interaction with either lignin or cellulose. Cations have a strong affinity towards hemicellulose, as it interacts strongly with the carboxylate group in hemicellulose. As the zoom levels while rendering the molecular structures were not the same, K^+ cation appears bigger than Na^+ and Cu^{2+} cations.

Demonstrating at a global scale that water reduces contacts with the surroundings by lubricating the cell wall interior, we again focus on the ions and what drives their differential diffusion. Figure 7 and supporting animations S4 – S6 illustrates as well as quantifies typical cation – cell

wall polymer interactions. When the water weight of the plant's secondary cell wall system increases, the contacts between cations and the cell wall polymers are generally reduced. In a solid system, the coordination number of the ions will be approximately constant, and thus the decrease in contacts to biopolymers leads to an increase in contacts to water molecules. For sodium or potassium (Figure 7D and E), the changes in contact number are monotonic. Similar trends where contacts are reduced at higher moisture levels are observed for Cu^{2+} interaction with cellulose and lignin, but not when interacting with hemicellulose (Figure 7F). Instead, we find that the reduction in number of contacts between the cation and hemicellulose is not monotonous. Instead, the cation-hemicellulose contacts increase beyond 15% water weight. We attribute this to the strong electrostatic interaction between the cation and carboxylate functional group in hemicellulose in our secondary cell wall model, with representative snapshots shown in Figures 7 A-C. We would anticipate that other divalent cations would have similar strong interactions with hemicellulose carboxylate groups and may need to be avoided when optimizing for diffusion within wood. Overall, for different salts used in this study, we find the cation interaction with hemicellulose is relatively stronger when compared to interactions with lignin or cellulose, due to the carboxylate functional group in hemicellulose.

4. Discussion

It is generally understood that diffusion through solid polymers including wood depends on molecular motions of the polymer, free volume in the polymer matrix, diffusant dimensions, and solubility of the diffusant in the polymer matrix (Engelund et al., 2013; Fredriksson et al., 2022). Diffusant transport is generally controlled by the motion of similar-sized features of the polymer matrix. Smaller diffusants, such as water molecules, are controlled by uncoordinated local motions, whereas larger chemicals, like mineral ions, are controlled by cooperative motions. As a hygroscopic material, water absorbs in the cell wall and acts as plasticizer that increases molecular motions and free volume. It is generally understood that diffusion is promoted by increases in water plasticization. Of particular interest is an ambient temperature moisture-induced glass transition that current evidence indicates occurs in the amorphous polysaccharides when wood is conditioned between 50 and 85% RH, which corresponds to 10-15% moisture content. Diffusion of larger chemicals, like mineral ions, are only expected to appreciably occur through rubbery polymers above their glass transition that have cooperative motions.

Within our simulations, where we identify a linear trend on a logarithmic scale (Figure 4), it would appear at first glance that we do not see a clear moisture-induced glass transition. However, if we replot Figure 4 on a linear scale (Figure 8), this same ion and polymer diffusion information shows a clear transition at between 10-15% moisture content, where the diffusion goes from effectively zero to growing approximately linearly. Based on this simplified depiction of the plant cell wall and the observation of piecewise linear ion and polymer diffusion, we suggest that below 15% water weight the system behaves as though it were effectively static. Above that moisture threshold, internal motions become appreciable, and the material transitions to a more “rubbery” state rather than a glass. This observation of a moisture-induced glass transition, based on diffusion coefficients calculated from atomistic simulations agrees well with previously reported XFM experiments (Jakes, 2019; Jakes et al., 2020, 2019). Below this threshold, the

diffusion for any permeant will be slow within a tightly bound arrangement of secondary cell wall biopolymers. However, once there is sufficient hydration, the diffusion approaches the maximum observed in an approximately linear fashion. Maintaining hydration above this transition point will be critical for applying penetrating treatments to woody biomass, and may contribute to vastly different cell wall diffusion measures across plant tissues (Kramer et al., 2007).

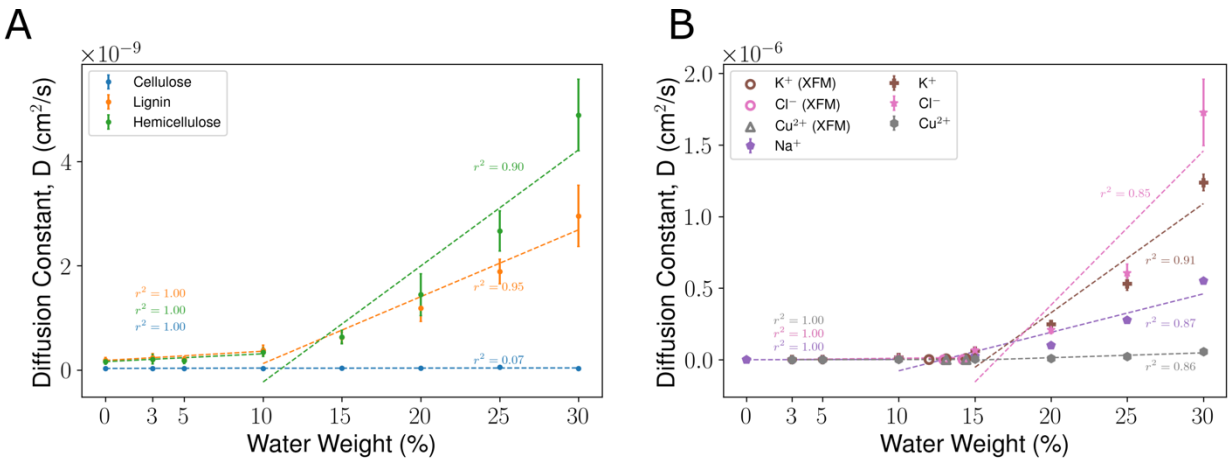

Figure 8: Diffusion of polymers and ions indicating a moisture dependent glass transition between 10 – 15 wt% water in plant secondary cell wall (A) for biopolymers cellulose, hemicellulose and lignin where diffusion constant is calculated using Einstein's relationship as described in Methods and Figure 4. (B) for monovalent cations (Na^+, K^+), monovalent anions (Cl^-) and divalent cations (Cu^{2+}). Ion diffusion in the plant secondary cell wall agrees well with previously reported X-ray fluorescence microscopy (XFM) experiments (Jakes et al., 2020).

Demonstrating this importance quantitatively, we can estimate the diffusion length and timescale for penetrating wood treatments, such as ions. For Fickian ion diffusion within in the secondary cell wall, the diffusion length for a given time is estimated by this formula: $L_D = \sqrt{2D\ t}$. Here, D is the diffusion coefficient and time t is how long one is willing to wait. Over short 50 ns timescales, Cu^{2+} has a corresponding diffusion length of less than 1 nm, even at the highest hydration level simulated. A single xylan monomer is about 0.9 nm large. Thus, divalent copper cations tend to remain bound to a single hemicellulose polymer in the cell wall for a considerable duration within our simulation. Similarly, for monovalent sodium and potassium cations, the diffusion lengths are less than 1 nm at below 15% water wt. and between 1 – 4 nm at higher levels of hydration in wood. Using these diffusion lengths, we estimate that treatments in dried wood would require timescales on the order of years to permeate 1 inch but may only take a month or two to diffuse within hydrated wood samples. In practice, where the initial concentration gradient is large rather than zero as it is in these simulations, practical treatments would take only hours in water-saturated wood.

The singular experience of how carboxylate groups on hemicellulose can impede divalent cation motion through strong ionic bonds illustrates potential strategies for modulating diffusion in woody tissues. For instance, modifying hemicellulose synthesis to eliminate carboxylates would

likely lead to accelerated cation diffusion, as the cations would not interact as strongly with a carbonyl or hydroxyl as they would with the carboxylate. Similarly, lignin acetylation would be expected to make lignin even more hydrophobic than it already is, altering transport dynamics (Hunt et al., 2018b). Further study on both the experimental and modeling frontiers will be needed to couple together cell wall chemistry to the impact on dynamics at the molecular level.

The ion diffusion results also have direct impact on the electrical conductivity of wood. Typical dried wood used as building materials is a good insulator. However, measured diffusions correlates with electrical conductivity of wood based on the Nernst-Einstein equation (Jakes et al., 2020). Thus, when an electric field is applied to wood with a moisture content above 10-15% or so, substantial ion diffusion may permit wood to act as a conductor, with conductivity spanning 6 orders of magnitude (Stamm, 1930). Increasing hydrophobicity of wood polymers, such as treatments via low molecular weight phenol-aldehyde resins to exclude water and thus reduce ion movement, would be expected to significantly reduce conductance.

5. Conclusion

Diffusion in plant cell wall is dependent on moisture levels. The diffusion of inorganic ions in plant cell wall measured from MD simulation increases with cell wall hydration, and agrees well with prior XFM experiments (Jakes et al., 2020). Diffusion for all species, but particularly K^+ and Cu^{2+} is observed to have a moisture-induced glass transition at 15% equilibrium moisture content in wood. Generally, cation diffusion within the cell wall is slower compared to anion diffusion, because of strong interactions between carboxylate groups on the hemicellulose and cation retard the free diffusion of positively charged permeants. Armed with this mechanism, it is possible to design and engineer pathways to alter the mechano-chemical properties of lignocellulosic biomass, catering to applications in sustainable, chemical, and biomedical engineering. The insights obtained from our molecular simulations provide key guidelines for future experimental and computational studies, where we anticipate extending this model to explore the effects of cell wall polymer heterogeneity and acetylation on the diffusivity and ionic conductivity in plant biomass at different hydration index.

The MD simulations further provide a detailed mechanistic view to relate moisture content to diffusive processes within plant secondary cell walls. One of the strongest conclusions is that the moisture-induced glass transition between at between 10 - 15 wt% water is a natural extension of existing trends in hydration space, where additional water facilitates polymer separation and ion solvation. Such quantitative and qualitative evaluation of molecular diffusion provides evidence towards the atomistic origins of cell wall being a barrier to diffusive transport, both for small and large diffusants, such as mineral ions and enzymes respectively. Hence strategies are being developed to engineer the cell wall microenvironment to ameliorate diffusion process, with an aim to create durable and sustainable plant-based biomaterials, to build a circular bioeconomy (Sheldon, 2020).

Acknowledgements

This work was performed as part of the Feedstock Conversion Interface Consortium (FCIC) with funding provided by the U.S. Department of Energy Bioenergy Technologies Office. This work was authored in part by Alliance for Sustainable Energy, LLC, the manager and operator of the National Renewable Energy Laboratory for the U.S. Department of Energy (DOE) under Contract No. DE-AC36-08GO28308. This work was supported in part through computational resources and services provided by the Institute for Cyber-Enabled Research at Michigan State University. The views expressed in the article do not necessarily represent the views of the DOE or the U.S. Government. The U.S. Government retains and the publisher, by accepting the article for publication, acknowledges that the U.S. Government retains a nonexclusive, paid-up, irrevocable, worldwide license to publish or reproduce the published form of this work, or allow others to do so, for U.S. Government purposes.

References

Arzola-Villegas, X., Lakes, R., Plaza, N.Z., Jakes, J.E., 2019. Wood Moisture-Induced Swelling at the Cellular Scale—Ab Intra. Forests 10, 996. https://doi.org/10.3390/f10110996

Autengruber, M., Lukacevic, M., Füssl, J., 2020. Finite-element-based moisture transport model for wood including free water above the fiber saturation point. Int. J. Heat Mass Transf. 161, 120228. https://doi.org/10.1016/j.ijheatmasstransfer.2020.120228

Beglov, D., Roux, B., 1994. Finite representation of an infinite bulk system: Solvent boundary potential for computer simulations. J. Chem. Phys. 100, 9050. https://doi.org/10.1063/1.466711

Brandner, R., Flatscher, G., Ringhofer, A., Schickhofer, G., Thiel, A., 2016. Cross laminated timber (CLT): overview and development. Eur. J. Wood Wood Prod. 74, 331–351. https://doi.org/10.1007/s00107-015-0999-5

Chen, Zhang, Shomali, Coasne, Carmeliet, Derome, 2019. Wood–Moisture Relationships Studied with Molecular Simulations: Methodological Guidelines. Forests 10, 628. https://doi.org/10.3390/f10080628

Cherubini, F., 2010. The biorefinery concept: Using biomass instead of oil for producing energy and chemicals. Energy Convers. Manag. 51, 1412–1421. https://doi.org/10.1016/j.enconman.2010.01.015

de Jong, E., Jungmeier, G., 2015. Biorefinery Concepts in Comparison to Petrochemical Refineries, in: Industrial Biorefineries & White Biotechnology. Elsevier, pp. 3–33. https://doi.org/10.1016/B978-0-444-63453-5.00001-X

Einstein, A., 1905. Über die von der molekularkinetischen Theorie der Wärme geforderte Bewegung von in ruhenden Flüssigkeiten suspendierten Teilchen. Ann. Phys. 322, 549–560. https://doi.org/10.1002/andp.19053220806

Engelund, E.T., Thygesen, L.G., Svensson, S., Hill, C.A.S., 2013. A critical discussion of the physics of wood–water interactions. Wood Sci. Technol. 47, 141–161. https://doi.org/10.1007/s00226-012-0514-7

Essmann, U., Perera, L., Berkowitz, M.L., Darden, T., Lee, H., Pedersen, L.G., 1995. A smooth particle mesh Ewald method. J. Chem. Phys. 103, 8577–8593. https://doi.org/10.1063/1.470117

Falk, B., 2009. Wood as a sustainable building material. For. Prod. J. v. 59, 6–12.

Feller, S.E., Zhang, Y., Pastor, R.W., Brooks, B.R., 1995. Constant pressure molecular dynamics simulation: The Langevin piston method. J. Chem. Phys. 103, 4613–4621. https://doi.org/10.1063/1.470648

Fredriksson, M., Rüggeberg, M., Nord-Larsen, T., Beck, G., Thybring, E.E., 2022. Water sorption in wood cell walls–data exploration of the influential physicochemical characteristics. Cellulose. https://doi.org/10.1007/s10570-022-04973-0

Glass, S.V., Zelinka, S.L., Johnson, J.A., 2014. Investigation of Historic Equilibrium Moisture Content Data from the Forest Products Laboratory (No. FPL-GTR-229). U.S. Department of Agriculture, Forest Service, Forest Products Laboratory, Madison, WI. https://doi.org/10.2737/FPL-GTR-229

Guvench, O., Greenr, S.N., Kamath, G., Brady, J.W., Venable, R.M., Pastor, R.W., Mackerell, A.D., 2008. Additive empirical force field for hexopyranose monosaccharides. J. Comput. Chem. 29, 2543–2564. https://doi.org/10.1002/jcc.21004

Guvench, O., Hatcher, E., Venable, R.M., Pastor, R.W., MacKerell, A.D., 2009. CHARMM Additive All-Atom Force Field for Glycosidic Linkages between Hexopyranoses. J. Chem. Theory Comput. 5, 2353–2370. https://doi.org/10.1021/ct900242e

Harris, C.R., Millman, K.J., van der Walt, S.J., Gommers, R., Virtanen, P., Cournapeau, D., Wieser, E., Taylor, J., Berg, S., Smith, N.J., Kern, R., Picus, M., Hoyer, S., van Kerkwijk, M.H., Brett, M., Haldane, A., del Río, J.F., Wiebe, M., Peterson, P., Gérard-Marchant, P., Sheppard, K., Reddy, T., Weckesser, W., Abbasi, H., Gohlke, C., Oliphant, T.E., 2020. Array programming with NumPy. Nature 585, 357–362. https://doi.org/10.1038/s41586-020-2649-2

Hatcher, E.R., Guvench, O., MacKerell, A.D., 2009. CHARMM Additive All-Atom Force Field for Aldopentofuranoses, Methyl-aldopentofuranosides, and Fructofuranose. J. Phys. Chem. B 113, 12466–12476. https://doi.org/10.1021/jp905496e

Hill, C.A.S., 2006. Wood Modification: Chemical, Thermal and Other Processes, 1st ed. Wiley. https://doi.org/10.1002/0470021748

Humphrey, W., Dalke, A., Schulten, K., 1996. VMD: Visual molecular dynamics. J. Mol. Graph. 14, 33–38. https://doi.org/10.1016/0263-7855(96)00018-5

Hunt, C.G., Frihart, C.R., Dunky, M., Rohumaa, A., 2018a. Understanding Wood Bonds–Going Beyond What Meets the Eye: A Critical Review. Rev. Adhes. Adhes. 6, 369–440. https://doi.org/10.7569/RAA.2018.097312

Hunt, C.G., Zelinka, S.L., Frihart, C.R., Lorenz, L., Yelle, D., Gleber, S.-C., Vogt, S., Jakes, J.E., 2018b. Acetylation increases relative humidity threshold for ion transport in wood cell walls – A means to understanding decay resistance. Int. Biodeterior. Biodegrad. 133, 230–237. https://doi.org/10.1016/j.ibiod.2018.06.014

Hunter, J.D., 2007. Matplotlib: A 2D Graphics Environment. Comput. Sci. Eng. 9, 90–95. https://doi.org/10.1109/MCSE.2007.55

Ibach, R.E., Plaza, N.Z., Pingali, S.V., 2022. Small Angle Neutron Scattering Reveals Wood Nanostructural Features in Decay Resistant Chemically Modified Wood. Front. For. Glob. Change 4, 814086. https://doi.org/10.3389/ffgc.2021.814086

Jakes, J.E., 2019. Mechanism for Diffusion through Secondary Cell Walls in Lignocellulosic Biomass. J. Phys. Chem. B 123, 4333–4339. https://doi.org/10.1021/acs.jpcb.9b01430

Jakes, J.E., Arzola, X., Bergman, R., Ciesielski, P., Hunt, C.G., Rahbar, N., Tshabalala, M., Wiedenhoeft, A.C., Zelinka, S.L., 2016. Not Just Lumber—Using Wood in the Sustainable Future of Materials, Chemicals, and Fuels. JOM 68, 2395–2404. https://doi.org/10.1007/s11837-016-2026-7

Jakes, J.E., Hunt, C.G., Zelinka, S.L., Ciesielski, P.N., Plaza, N.Z., 2019. Effects of Moisture on Diffusion in Unmodified Wood Cell Walls: A Phenomenological Polymer Science Approach. Forests 10, 1084. https://doi.org/10.3390/f10121084

Jakes, J.E., Zelinka, S.L., Hunt, C.G., Ciesielski, P., Frihart, C.R., Yelle, D., Passarini, L., Gleber, S.-C., Vine, D., Vogt, S., 2020. Measurement of moisture-dependent ion diffusion constants in wood cell wall layers using time-lapse micro X-ray fluorescence microscopy. Sci. Rep. 10, 9919. https://doi.org/10.1038/s41598-020-66916-8

Jorgensen, W.L., Chandrasekhar, J., Madura, J.D., Impey, R.W., Pastor, M.L., 1983. COMPARISON OF SIMPLE POTENTIAL FUNCTIONS FOR SIMULATING LIQUID WATER. J Chem Phys 79, 926–935. https://doi.org/10.1063/1.445869

Kirker, G., Zelinka, S., Gleber, S.-C., Vine, D., Finney, L., Chen, S., Hong, Y.P., Uyarte, O., Vogt, S., Jellison, J., Goodell, B., Jakes, J.E., 2017. Synchrotron-based X-ray fluorescence microscopy enables multiscale spatial visualization of ions involved in fungal lignocellulose deconstruction. Sci. Rep. 7, 41798. https://doi.org/10.1038/srep41798

Kirker, G.T., Lebow, S.T., 2021. Wood preservatives, in: Wood Handbook: Wood as an Engineering Material. U.S. Department of Agriculture, Forest Service, Forest Products Laboratory, Madison, WI, p. 26.

Kirui, A., Zhao, W., Deligey, F., Yang, H., Kang, X., Mentink-Vigier, F., Wang, T., 2022. Carbohydrate-aromatic interface and molecular architecture of lignocellulose. Nat. Commun. 13, 538. https://doi.org/10.1038/s41467-022-28165-3

Kothari, N., Holwerda, E.K., Cai, C.M., Kumar, R., Wyman, C.E., 2018. Biomass augmentation through thermochemical pretreatments greatly enhances digestion of switchgrass by Clostridium thermocellum. Biotechnol. Biofuels 11, 219. https://doi.org/10.1186/s13068-018-1216-7

Kramer, E.M., Frazer, N.L., Baskin, T.I., 2007. Measurement of diffusion within the cell wall in living roots of Arabidopsis thaliana. J. Exp. Bot. 58, 3005–3015. https://doi.org/10.1093/jxb/erm155

Langan, P., Sukumar, N., Nishiyama, Y., Chanzy, H., 2005. Synchrotron X-ray structures of cellulose Iβ and regenerated cellulose II at ambient temperature and 100 K. Cellulose 12, 551–562. https://doi.org/10.1007/s10570-005-9006-3

Lyczakowski, J.J., Bourdon, M., Terrett, O.M., Helariutta, Y., Wightman, R., Dupree, P., 2019. Structural Imaging of Native Cryo-Preserved Secondary Cell Walls Reveals the Presence of Macrofibrils and Their Formation Requires Normal Cellulose, Lignin and Xylan Biosynthesis. Front. Plant Sci. 10, 1398. https://doi.org/10.3389/fpls.2019.01398

Mark, P., Nilsson, L., 2001. Structure and Dynamics of the TIP3P, SPC, and SPC/E Water Models at 298 K. J. Phys. Chem. A 105, 9954–9960. https://doi.org/10.1021/jp003020w

Martínez, L., Andrade, R., Birgin, E.G., Martínez, J.M., 2009. PACKMOL: A package for building initial configurations for molecular dynamics simulations. J. Comput. Chem. 30, 2157–2164. https://doi.org/10.1002/jcc.21224

Miyamoto, S., Kollman, P. a, 1992. SETTLE: an analytical version of the SHAKE and RATTLE algorithm for rigid water models. J. Comput. Chem. 13, 952–962. https://doi.org/10.1002/jcc.540130805

Mosier, N., Wyman, C., Dale, B., Elander, R., Lee, Y., Holtzapple, M., Ladisch, M., 2005. Features of promising technologies for pretreatment of lignocellulosic biomass. Bioresour. Technol. 96, 673–686. https://doi.org/10.1016/j.biortech.2004.06.025

Paajanen, A., Zitting, A., Rautkari, L., Ketoja, J.A., Penttilä, P.A., 2022. Nanoscale Mechanism of Moisture-Induced Swelling in Wood Microfibril Bundles. Nano Lett. 22, 5143–5150. https://doi.org/10.1021/acs.nanolett.2c00822

Paterlini, M.G., Ferguson, D.M., 1998. Constant temperature simulations using the Langevin equation with velocity Verlet integration. Chem. Phys. 236, 243–252. https://doi.org/10.1016/S0301-0104(98)00214-6

Perras, F.A., Luo, H., Zhang, X., Mosier, N.S., Pruski, M., Abu-Omar, M.M., 2017. Atomic-Level Structure Characterization of Biomass Pre- and Post-Lignin Treatment by Dynamic Nuclear Polarization-Enhanced Solid-State NMR. J. Phys. Chem. A 121, 623–630. https://doi.org/10.1021/acs.jpca.6b11121

Phillips, J.C., Hardy, D.J., Maia, J.D.C., Stone, J.E., Ribeiro, J.V., Bernardi, R.C., Buch, R., Fiorin, G., Hénin, J., Jiang, W., McGreevy, R., Melo, M.C.R., Radak, B.K., Skeel, R.D., Singharoy, A., Wang, Y., Roux, B., Aksimentiev, A., Luthey-Schulten, Z., Kalé, L.V., Schulten, K., Chipot, C., Tajkhorshid, E., 2020. Scalable molecular dynamics on CPU and GPU architectures with NAMD. J. Chem. Phys. 153, 044130. https://doi.org/10.1063/5.0014475

Plaza, N.Z., Pingali, S.V., Ibach, R.E., 2022. Nanostructural Changes Correlated to Decay Resistance of Chemically Modified Wood Fibers. Fibers 10, 40. https://doi.org/10.3390/fib10050040

Plaza Rodriguez, N.Z., 2017. Neutron Scattering Studies of Nano-Scale Wood-Water Interactions (Thesis). University of Wisconsin-Madison, Madison, WI.

Ralph, J., Lapierre, C., Boerjan, W., 2019. Lignin structure and its engineering. Curr. Opin. Biotechnol. 56, 240–249. https://doi.org/10.1016/j.copbio.2019.02.019

Sheinerman, F.B., Brooks, C.L., 1998. Calculations on folding of segment B1 of streptococcal protein G. J. Mol. Biol. 278, 439–456. https://doi.org/10.1006/jmbi.1998.1688

Sheldon, R.A., 2020. Biocatalysis and biomass conversion: enabling a circular economy. Philos. Trans. R. Soc. Math. Phys. Eng. Sci. 378, 20190274. https://doi.org/10.1098/rsta.2019.0274

Shi, J., Avramidis, S., 2021. Nanopore-Level Wood-Water Interactions—A Molecular Simulation Study. Forests 12, 356. https://doi.org/10.3390/f12030356

Stamm, A.J., 1930. An Electrical Conductivity Method for Determining the Moisture Content of Wood. Ind. Eng. Chem. Anal. Ed. 2, 240–244. https://doi.org/10.1021/ac50071a012

Thornburg, N.E., Pecha, M.B., Brandner, D.G., Reed, M.L., Vermaas, J.V., Michener, W.E., Katahira, R., Vinzant, T.B., Foust, T.D., Donohoe, B.S., Román-Leshkov, Y., Ciesielski, P.N.,

Beckham, G.T., 2020. Mesoscale Reaction–Diffusion Phenomena Governing Lignin-First Biomass Fractionation. ChemSusChem 13, 4495–4509. https://doi.org/10.1002/cssc.202000558

Vermaas, J.V., Petridis, L., Ralph, J., Crowley, M.F., Beckham, G.T., 2019. Systematic parameterization of lignin for the CHARMM force field. Green Chem. 21, 109–122. https://doi.org/10.1039/C8GC03209B

Virtanen, P., Gommers, R., Oliphant, T.E., Haberland, M., Reddy, T., Cournapeau, D., Burovski, E., Peterson, P., Weckesser, W., Bright, J., van der Walt, S.J., Brett, M., Wilson, J., Millman, K.J., Mayorov, N., Nelson, A.R.J., Jones, E., Kern, R., Larson, E., Carey, C.J., Polat, İ., Feng, Y., Moore, E.W., VanderPlas, J., Laxalde, D., Perktold, J., Cimrman, R., Henriksen, I., Quintero, E.A., Harris, C.R., Archibald, A.M., Ribeiro, A.H., Pedregosa, F., van Mulbregt, P., SciPy 1.0 Contributors, Vijaykumar, A., Bardelli, A.P., Rothberg, A., Hilboll, A., Kloeckner, A., Scopatz, A., Lee, A., Rokem, A., Woods, C.N., Fulton, C., Masson, C., Häggström, C., Fitzgerald, C., Nicholson, D.A., Hagen, D.R., Pasechnik, D.V., Olivetti, E., Martin, E., Wieser, E., Silva, F., Lenders, F., Wilhelm, F., Young, G., Price, G.A., Ingold, G.-L., Allen, G.E., Lee, G.R., Audren, H., Probst, I., Dietrich, J.P., Silterra, J., Webber, J.T., Slavič, J., Nothman, J., Buchner, J., Kulick, J., Schönberger, J.L., de Miranda Cardoso, J.V., Reimer, J., Harrington, J., Rodríguez, J.L.C., Nunez-Iglesias, J., Kuczynski, J., Tritz, K., Thoma, M., Newville, M., Kümmerer, M., Bolingbroke, M., Tartre, M., Pak, M., Smith, N.J., Nowaczyk, N., Shebanov, N., Pavlyk, O., Brodtkorb, P.A., Lee, P., McGibbon, R.T., Feldbauer, R., Lewis, S., Tygier, S., Sievert, S., Vigna, S., Peterson, S., More, S., Pudlik, T., Oshima, T., Pingel, T.J., Robitaille, T.P., Spura, T., Jones, T.R., Cera, T., Leslie, T., Zito, T., Krauss, T., Upadhyay, U., Halchenko, Y.O., Vázquez-Baeza, Y., 2020. SciPy 1.0: fundamental algorithms for scientific computing in Python. Nat. Methods 17, 261–272. https://doi.org/10.1038/s41592-019-0686-2

Walker, J.C.F., 2006. Basic wood chemistry and cell wall ultrastructure, in: Primary Wood Processing. Springer Netherlands, pp. 23–67. https://doi.org/10.1007/1-4020-4393-7_2

Xu, H., Li, B., Mu, X., 2016. Review of Alkali-Based Pretreatment To Enhance Enzymatic Saccharification for Lignocellulosic Biomass Conversion. Ind. Eng. Chem. Res. 55, 8691–8705. https://doi.org/10.1021/acs.iecr.6b01907

Zauer, M., Pfriem, A., Wagenführ, A., 2013. Toward improved understanding of the cell-wall density and porosity of wood determined by gas pycnometry. Wood Sci. Technol. 47, 1197–1211. https://doi.org/10.1007/s00226-013-0568-1

Zelinka, S.L., Gleber, S.-C., Vogt, S., Rodríguez López, G.M., Jakes, J.E., 2015. Threshold for ion movements in wood cell walls below fiber saturation observed by X-ray fluorescence microscopy (XFM). Holzforschung 69, 441–448. https://doi.org/10.1515/hf-2014-0138

Zelinka, S.L., Jakes, J.E., Kirker, G.T., Passarini, L., Hunt, C.G., Lai, B., Antipova, O., Li, L., Vogt, S., 2019. Copper distribution and oxidation states near corroded fasteners in treated wood. SN Appl. Sci. 1, 240. https://doi.org/10.1007/s42452-019-0249-2

Zelinka, S.L., Sichel, R.J., Stone, D.S., 2010. Exposure testing of fasteners in preservative treated wood: Gravimetric corrosion rates and corrosion product analyses. Corros. Sci. 52, 3943–3948. https://doi.org/10.1016/j.corsci.2010.08.014

Zhu, H., Luo, W., Ciesielski, P.N., Fang, Z., Zhu, J.Y., Henriksson, G., Himmel, M.E., Hu, L., 2016. Wood-Derived Materials for Green Electronics, Biological Devices, and Energy

Applications. Chem. Rev. 116, 9305–9374.
https://doi.org/10.1021/acs.chemrev.6b00225

SI

The supporting information includes supplementary animations. In Animation S1, we show a periodic visualization for our cell wall model, highlighting the density of the cellulose (blue), lignin (orange), and hemicellulose (green) components. In Animation S2, we visualize a single simulation unit cell at 5% hydration using the same coloration scale, whereas Animation S3 visualizes the 30% hydration simulation. Animation S4, S5, and S6 show sodium, potassium and copper ions diffusing around the central cellulose fibril (blue), along with nearby carboxylated hemicellulose units.